Floquet scattering through a parity–time symmetric oscillating potential

Xuzhen Cao(曹序桢)[1,2], Zhaoxin Liang(梁兆新)[3,†], and Ying Hu(胡颖)[1,2,‡]

[1] *State Key Laboratory of Quantum Optics and Quantum Optics Devices, Institute of Laser Spectroscopy, Shanxi University, Taiyuan* 030006, *China*
[2] *Collaborative Innovation Center of Extreme Optics, Shanxi University, Taiyuan* 030006, *China*
[3] *Department of Physics, Zhejiang Normal University, Jinhua* 321004, *China*

(Received 21 September 2022; revised manuscript received 9 November 2022; accepted manuscript online 17 November 2022)

We investigate the scattering of a particle from a trapping potential that is subjected to weak, parity–time symmetric periodic drivings. Using the Floquet theory, we derive the scattering matrix and calculate the transmittance of the incident particle. When the driving is purely coherent, our calculation recovers the known result and the transmission spectrum shows the familiar, bound-state-induced Fano resonances. When the driving is purely incoherent, we find the Fano resonances still occur, but the lineshape of each resonance is reversed compared to the coherent-driving counterpart. Intriguingly, the transmission resonances disappear when both the coherent and incoherent driving fields are present with equal amplitudes. This phenomena can be seen as a manifestation of the non-reciprocal coupling of Floquet channels in the frequency domain. Notably, when the frequency up-conversion is absent, the transmission is such as if there is no driving at all, even when the driving strength increases.

Keywords: open system, periodic driving, scattering

PACS: 03.65.Yz, 03.65.–w, 03.65.Nk **DOI:** 10.1088/1674-1056/aca39a

1. Introduction

Quantum mechanics postulates the Hermiticity of the Hamiltonian operator, which ensures real eigen-energies. Open systems, however, are usually associated with non-Hermitian Hamiltonians exhibiting complex eigenenergies. In the seminal work,[1] Bender and Boettcher pointed out that if a non-Hermitian Hamiltonian is invariant under the combined parity and time-reversal operations, it can also exhibit entirely real spectra under certain conditions. Such parity–time reflection symmetric ($\mathcal{PT}$-symmetric) Hamiltonian can describe, for instance, an open system with balanced loss and gain. Over the past few years, there have been significant interests and ongoing efforts in exploring the $\mathcal{PT}$-symmetric systems. A plethora of novel phenomena with non-Hermitian analogue have been predicted, such as the $\mathcal{PT}$ phase transition, exceptional points and related topological phenomena; see review[2] and references therein. Notably, with the advance in engineering gain and loss, $\mathcal{PT}$-symmetric physics have been realized and applied in various settings, including mechanical[3] and optical platforms,[4–8] cavity systems,[9,10] lasers,[11,12] and optomechanical systems.[13–16]

Here, we study the systems that are subjected to $\mathcal{PT}$-symmetric periodic driving fields, aiming at the scattering behavior in such setups. In the Hermitian case, the study of scattering has played an important role both in the fundamental physics and in practical applications. We specifically study the scattering of particle in a one-dimensional (1D) continuous model where the scattering potential is subjected to $\mathcal{PT}$-symmetric drivings. Such a setup, when the driving is absent, has been a paradigm for exploring the scattering problem. In the presence of a coherent time-periodic field, the transport phenomena has also been well studied.[17–23] The key physics introduced by the coherent oscillating field is that the scattering involves multi-channel processes, *i.e.*, not only through elastic process, but also inelastic processes involving the absorption and emission of the energy quanta from the oscillating field. This results in important phenomena such as Fano resonance and quasi-bound states,[23] photon-assisted tunneling observed in quantum dots and superlattices,[24–27] and resonance catastrophe.[28] The purpose of this work is to explore how the transmission property is affected by the non-Hermiticity of the driving fields. In particular, adding an incoherent driving on top of the coherent driving field may break the reciprocity of coupling between Floquet channels in the frequency domain, which is expected to enrich the scattering physics.

The non-Hermitian scattering has been previously studied in tight-binding lattice models.[29–31] There, it has been shown that the interplay between the energy band (gap) of the lattice structure and the non-Hermitian driving gives rise to some exotic transport behavior such as the non-Hermitian Floquet invisibility.[30] Here, we show that non-Hermitian driving can induce intriguing scattering phenomena already in a continuous model.

†Corresponding author. E-mail: zhxliang@zjnu.edu.cn
‡Corresponding author. E-mail: huying@sxu.edu.cn

© 2023 Chinese Physical Society and IOP Publishing Ltd

Specifically, we derive the scattering matrix and calculate the transmission spectrum of the incident particle, based on the Floquet theory[32] and the extension of the approach in Ref. [23] to the non-Hermitian driving case. When the driving is purely coherent, the transmission spectrum shows the well known, bound-state induced Fano resonances. In contrast, when the driving is purely incoherent, we find that, while Fano resonances of the same origin still appear in the transmission spectrum, the lineshape of each resonance is reversed compared to the coherent-driving counterpart. Interestingly, we find the transmission resonances disappear in the combined presence of coherent and incoherent time-periodic fields of equal amplitudes. This phenomenon is a manifestation of the nonreciprocal coupling of Floquet channels in the frequency domain. Depending on the nonreciprocal direction, the transmissions show different behavior: when the frequency up-conversion is absent, the particle transmits in such a way as if there is no driving at all, even when the driving strength increases. On the other hand, if the frequency down-conversion is absent, the transmission is enhanced with the increase of the driving strength. These results further our understanding of the transport properties in the presence of non-Hermitian periodic drivings.

2. Model system

We consider a setup as illustrated in Fig. 1, where a propagating particle is transmitting through a non-Hermitian oscillating square potential in one dimension. The time evolution of the particle's wavefunction $\psi(x,t)$ is governed by the Schrödinger equation

$$\mathrm{i}\hbar\frac{\partial\psi(x,t)}{\partial t}=-\frac{\hbar^2}{2\mu}\frac{\partial^2\psi(x,t)}{\partial x^2}+V(x,t)\psi(x,t). \tag{1}$$

Here, $\hbar$ is the Planck constant, μ is the mass of the particle, and $V(x,t)$ is a time-dependent non-Hermitian potential in the form

$$V(x,t)=\begin{cases}0, & |x|>L/2,\\ V_0+V_1\cos\omega t-\mathrm{i}V_2\sin\omega t, & |x|\le L/2.\end{cases} \tag{2}$$

In Eq. (2), $V_\alpha\in\mathcal{R}$ are real numbers ($\alpha=0,1,2$); specifically, V_0 is the amplitude of static potential, while V_1 and V_2 denote the amplitudes of coherent and incoherent periodic drivings, respectively. The coherent and incoherent driving fields have the same driving frequency ω, so $V(x,t)=V(x,t+2\pi/\omega)$ with the period $2\pi/\omega$. The non-Hermitian Hamiltonian in Eq. (1) is $\mathcal{PT}$-symmetric. To see this, we directly apply the parity operator of $\mathcal{P}$ and time operator of $\mathcal{T}$ on Eq. (2) and calculate

$$\begin{aligned}&\mathcal{PT}^{-1}V(x,t)\mathcal{PT}=V_0+V_1\cos\left[\omega\left(\mathcal{T}^{-1}t\mathcal{T}\right)\right]\\&-(\mathcal{T}^{-1}\mathrm{i}\mathcal{T})V_2\sin\left[\omega(\mathcal{T}^{-1}t\mathcal{T})\right]=V(x,t)\end{aligned} \tag{3}$$

by virtual of $\mathcal{T}^{-1}t\mathcal{T}=-t$ and $\mathcal{T}^{-1}\mathrm{i}\mathcal{T}=-\mathrm{i}$, thus proving the $\mathcal{PT}$ symmetry of the Hamiltonian. Our goal is to investigate the transmittance of the particle through the non-Hermitian oscillating potential.

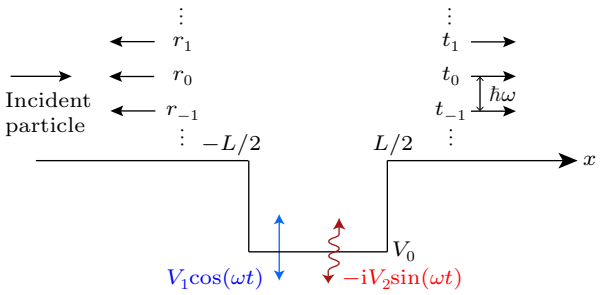


Fig. 1. Schematic diagram of Floquet scattering of a particle from a non-Hermitian oscillating potential. The incident particle interacts with an oscillating potential of the form $V(x,t)=V_0+V_1\cos\omega t-\mathrm{i}V_2\sin\omega t$ in the regime $x\in[-L/2,L/2]$. Here V_0 is the amplitude of the static potential, V_1 (V_2) is the coherent (incoherent) driving amplitude, and ω is the driving frequency. Transmission (with an amplitude t_n) and reflection (with an amplitude r_n) in the Floquet channel $E_n=\varepsilon+n\hbar\omega$ ($n=-\infty,\ldots,\infty$) is illustrated.

The system described above in the absence of periodic modulations ($V_1=V_2=0$) provides a textbook example for the exploration of the particle scattering. Cases with a coherent periodic driving field (*i.e.*, $V_1\neq0$ and $V_2=0$) have also been well studied.[17–23] There, due to the oscillating field, propagating particles can transmit through multiple channels, not only through elastic process, but also via inelastic processes, namely the absorption or emission of energy quanta from the driving field. Below we extend these studies and techniques beyond the Hermitian realm, and consider the addition of a weak, incoherent driving field, *i.e.*, $|V_2|<|V_0|$. In practice, such a term can result from, for instance, a periodic gain (*e.g.*, an incoherent pump) and loss.

3. Floquet scattering matrix for $\mathcal{PT}$-symmetric-driven potential

To study the scattering behavior of the particle interacting with the non-Hermitian, driven potential, we rely on the Floquet theory[32] to derive the scattering matrix, along the line of Ref. [23].

We begin by writing the solution to Eq. (1) as

$$\psi(x,t)=\mathrm{e}^{-\mathrm{i}\varepsilon t/\hbar}\phi(x,t), \tag{4}$$

where $\phi(x,t)=\phi(x,t+2\pi/\omega)=\sum_n\phi_n\exp(-\mathrm{i}n\omega t)$ is the so-called Floquet state. In Eq. (4), ε is the quasienergy, which in general is complex valued for $V_2\neq0$. Substituting Eq. (4) into Eq. (1), we obtain the Floquet eigenvalue equation

$$-\mathrm{i}\hbar\frac{\partial\phi}{\partial t}-\frac{\hbar^2}{2\mu}\frac{\partial^2\phi}{\partial x^2}+V(x,t)\phi=\varepsilon\phi. \tag{5}$$

For the $\mathcal{PT}$-symmetric system described in Eq. (1), we are interested in the regime where $\varepsilon\in R$ is entirely real. Since

ε is defined up to integer multiples of $\hbar\omega$, we restrict the computation to the first Brillouin zone $|\varepsilon| < \hbar\omega$. Considering the potential $V(x,t)$ in Eq. (2) is a piecewise function in space, below we solve Eq. (5) for $\phi(x,t)$ separately in three regions, namely $x < -L/2$, $|x| < L/2$, and $x > L/2$; matching these solutions at the boundaries will provide us the desired scattering matrix.

In the regions $|x| > L/2$, we have $V(x,t) = 0$ and $\phi(x,t)$ can be easily solved. The general solutions are

$$\phi = \sum_{n=-\infty}^{\infty} \left(A_n^{\mathrm{i}} \mathrm{e}^{\mathrm{i}k_n x} + A_n^{\mathrm{o}} \mathrm{e}^{-\mathrm{i}k_n x}\right) \mathrm{e}^{-\mathrm{i}n\omega t}, \quad (x < -L/2), \tag{6}$$

$$\phi = \sum_{n=-\infty}^{\infty} \left(B_n^{\mathrm{i}} \mathrm{e}^{-\mathrm{i}k_n x} + B_n^{\mathrm{o}} \mathrm{e}^{\mathrm{i}k_n x}\right) \mathrm{e}^{-\mathrm{i}n\omega t}, \quad (x > L/2), \tag{7}$$

with $k_n = \sqrt{2\mu(\varepsilon + n\hbar\omega)}/\hbar$. Here A_n^{i} (B_n^{i}) labels the amplitude of the incoming plane wave from the left (right) in the n-th Floquet channel. Note that if $\varepsilon + n\hbar\omega < 0$, k_n becomes imaginary, namely the corresponding channel supports an evanescent mode localized in space, instead of a propagating mode. Moreover, the A_n^{o} (B_n^{o}) describes the amplitude of the reflected (transmitted) wave after the scattering of the particle off the oscillating potential.

In the region $|x| < L/2$, where the potential $V(x,t)$ exists, we solve Eq. (5) by separating the variables $\phi(x,t) = g(x)f(t)$, with $f(t + 2\pi/\omega) = f(t)$. We obtain

$$\mathrm{i}\hbar\frac{\partial f}{\partial t} - [V_1\cos(\omega t) - \mathrm{i}V_2\sin(\omega t)]f = (E-\varepsilon)f, \tag{8}$$

$$-\frac{\hbar^2}{2\mu}\frac{\partial^2 g}{\partial x^2} + V_0 g = Eg, \tag{9}$$

with the constant E introduced during the variable separations. Equation (8) can be directly solved by integrating over time, yielding

$$f(t) = \exp[-\mathrm{i}(E-\varepsilon)t/\hbar] \times \exp\left[-\mathrm{i}\frac{V_1}{\hbar\omega}\sin(\omega t) + \frac{V_2}{\hbar\omega}(\cos(\omega t) - 1)\right], \tag{10}$$

where we have used $f(0) = 1$. For our purpose it is useful to make Fourier expansions of Eq. (10) and write

$$f(t) = \mathrm{e}^{-\mathrm{i}(E-\varepsilon)t/\hbar}\mathrm{e}^{-V_2/\hbar\omega} \times \sum_{n=-\infty}^{\infty}\sum_{l=-\infty}^{\infty} \mathrm{i}^l \mathrm{J}_n\left(\frac{V_1}{\hbar\omega}\right)\mathrm{J}_l\left(-\mathrm{i}\frac{V_2}{\hbar\omega}\right)\mathrm{e}^{-\mathrm{i}(n-l)\omega t},$$

where we have used the identity $\exp(\mathrm{i}x\sin\theta) = \sum_n \mathrm{J}_n(x)\exp(\mathrm{i}n\theta)$, with $\mathrm{J}_n(x)$ the n-th order Bessel function of the first kind. The time-periodicity of $f(t)$ imposes the condition $E = \varepsilon + m\hbar\omega$. As such, the general solution to Eq. (9) can be written as $g(x) = \sum_{m=-\infty}^{\infty}(a_m \mathrm{e}^{\mathrm{i}q_m x} + b_m \mathrm{e}^{-\mathrm{i}q_m x})$ with a_m and b_m the coefficients, and $q_m = \sqrt{2\mu(\varepsilon + m\hbar\omega - V_0)}/\hbar$. Collecting the results for $g(x)$ and $f(t)$, we obtain $\phi(x,t)$ as

$$\phi = \sum_{m,n=-\infty}^{\infty}\left(a_m \mathrm{e}^{\mathrm{i}q_m x} + b_m \mathrm{e}^{-\mathrm{i}q_m x}\right) h_{n-m}\mathrm{e}^{-\mathrm{i}n\omega t}. \tag{11}$$

where we have introduced

$$h_{n-m} = \exp\left(-\frac{V_2}{\hbar\omega}\right)\sum_{l=-\infty}^{\infty}\mathrm{i}^l \mathrm{J}_{n-m+l}\left(\frac{V_1}{\hbar\omega}\right)\mathrm{J}_l\left(-\mathrm{i}\frac{V_2}{\hbar\omega}\right). \tag{12}$$

Matching Eqs. (6), (7), and (11) at the boundaries, we now derive the scattering matrix. Specifically, at $x = -L/2$, we obtain from the continuity conditions that

$$\begin{aligned} & A_n^{\mathrm{i}}\mathrm{e}^{-\mathrm{i}k_n L/2} + A_n^{\mathrm{o}}\mathrm{e}^{\mathrm{i}k_n L/2} \\ = & \sum_{m=-\infty}^{\infty}(a_m \mathrm{e}^{-\mathrm{i}q_m L/2} + b_m \mathrm{e}^{\mathrm{i}q_m L/2})h_{n-m}, \\ & \mathrm{i}k_n(A_n^{\mathrm{i}}\mathrm{e}^{-\mathrm{i}k_n L/2} - A_n^{\mathrm{o}}\mathrm{e}^{\mathrm{i}k_n L/2}) \\ = & \sum_{m=-\infty}^{\infty}\mathrm{i}q_m(a_m \mathrm{e}^{-\mathrm{i}q_m L/2} - b_m \mathrm{e}^{\mathrm{i}q_m L/2})h_{n-m}. \end{aligned} \tag{13}$$

Similarly, at $x = L/2$, we have

$$\begin{aligned} & B_n^{\mathrm{i}}\mathrm{e}^{-\mathrm{i}k_n L/2} + B_n^{\mathrm{o}}\mathrm{e}^{\mathrm{i}k_n L/2} \\ = & \sum_{m=-\infty}^{\infty}(a_m \mathrm{e}^{\mathrm{i}q_m L/2} + b_m \mathrm{e}^{-\mathrm{i}q_m L/2})h_{n-m}, \\ & -\mathrm{i}k_n(B_n^{\mathrm{i}}\mathrm{e}^{-\mathrm{i}k_n L/2} - B_n^{\mathrm{o}}\mathrm{e}^{\mathrm{i}k_n L/2}) \\ = & \sum_{m}^{\infty}\mathrm{i}q_m(a_m \mathrm{e}^{\mathrm{i}q_m L/2} - b_m \mathrm{e}^{-\mathrm{i}q_m L/2})h_{n-m}. \end{aligned} \tag{14}$$

Eliminating a_m and b_m in Eqs. (13) and (14), as detailed in the Appendix A, we arrive at

$$\begin{pmatrix} \boldsymbol{A}^{\mathrm{o}} \\ \boldsymbol{B}^{\mathrm{o}} \end{pmatrix} = \boldsymbol{S}\begin{pmatrix} \boldsymbol{A}^{\mathrm{i}} \\ \boldsymbol{B}^{\mathrm{i}} \end{pmatrix}, \tag{15}$$

with the scattering matrix

$$\boldsymbol{S} \equiv \begin{pmatrix} \boldsymbol{R} & \boldsymbol{T}' \\ \boldsymbol{T} & \boldsymbol{R}' \end{pmatrix}.$$

In Eq. (15), the vector $\boldsymbol{A}^{\mathrm{i}} = [\ldots A_{-1}^{\mathrm{i}}, A_0^{\mathrm{i}}, A_1^{\mathrm{i}}\ldots]^{\mathrm{T}}$ ($\boldsymbol{B}^{\mathrm{i}} = [\ldots B_{-1}^{\mathrm{i}}, B_0^{\mathrm{i}}, B_1^{\mathrm{i}}\ldots]^{\mathrm{T}}$) denotes the incident amplitudes from the left (right) in Floquet channels, $\boldsymbol{A}^{\mathrm{o}}$ and $\boldsymbol{B}^{\mathrm{o}}$ denote the corresponding reflected and transmitted parts of the scattered waves. In the scattering matrix $\boldsymbol{S}$, $\boldsymbol{R}$, and $\boldsymbol{T}$ ($\boldsymbol{R}'$ and $\boldsymbol{T}'$) denote the transmission and reflection matrices for a particle incident from the left (right). Specifically, the matrix element t_{nm} (r_{nm}) represents the amplitude of the transmitted (reflected) wave in the n-th Floquet channel for the incoming wave in the m-th channel. Detailed derivations for $\boldsymbol{S}$ is shown in Appendix A.

Without loss of generality, we assume the particle is incident from the left with the energy $E_0 = \varepsilon$ (thus $E_0/(\hbar\omega) \leq 1$), so that $A_n^{\mathrm{i}} = \delta_{n,0}^{\mathrm{i}}$ and $B_n^{\mathrm{i}} = 0$. Using Eq. (15), the transmittance T of the particle, *i.e.*, its total transmission amplitude can be calculated as

$$T = \sum_n \frac{k_n}{k_0}|t_{n0}|^2. \tag{16}$$

Here the summation is performed over all Floquet channels involving propagating modes (*i.e.*, $k_n \in \mathcal{R}$), whereas the localized, evanescent modes (*i.e.*, modes with $\mathrm{Im}(k_n) \neq 0$) do not contribute to T and are excluded.

Equation (16) is the central equation for our subsequent analysis of the transmission of a particle, in particular, we will elucidate the role of non-Hermitian driving (*i.e.*, $iV_2\sin(\omega t)$ by comparing the transmission in the presence and absence of non-Hermitian driving field. We will assume $V_0 < 0$ corresponding to a trapping potential, where bound states with the energy $E_b < 0$ can exist without external driving. Moreover, we restrict ourselves to the weak driving regimes where $|V_{1(2)}| < |V_0|$ and $|V_{1(2)}|/(\hbar\omega) \leq 1$. Note that all energy scales will be in the unit of $E_R = \hbar^2/(2\mu a^2)$ with a being a typical length unit of the system. In addition, in our numerical calculations we only take into account of a finite number of Floquet channels; where to truncate is determined from the evaluation of the Bessel function.

4. Scattering from a coherently driven potential

To benchmark our subsequent calculations, we start with considering $V_1 \neq 0$ and $V_2 = 0$, corresponding to a Hermitian oscillating potential,[23] and derive the particle transmission. In Fig. 2(a), we take $V_0 = -E_R$, $V_1 = 0.1E_R$, and $\hbar\omega = E_R$, and show the transmittance T as a function of the incident particle's energy E_0. The transmission spectrum in Fig. 2(a) features a Fano resonance with an asymmetric lineshape,[33] where a dip is followed by a peak (see the inset of Fig. 2(a)).

The Fano resonance occurs due to the resonant transitions between the incident channel and the bound state via the absorption and emission of energy quanta. For the chosen parameter, there exists one bound state with $E_b \approx -0.19\hbar\omega$ in the absence of driving (see Apendix B), which is within the energy range $[-\hbar\omega, 0]$. Thus a resonance occurs when $E_0 - \hbar\omega = E_b$, *i.e.*, the incident particle emits one energy quanta $\hbar\omega$ and jumps to the bound state with the energy $E_b < 0$, which does not contribute to the transmission, giving rise to a dip in the spectrum; reciprocally, a particle in the bound state can absorb one energy quanta and be excited to the incident channel, thus transmitting through. The resonance with the bound state via emitting $\hbar\omega$ is evidenced in Fig. 2(b). There, we plot the transmission probability $|t_{-10}|^2$ as a function of $E_0/(\hbar\omega)$. The singularity at $E_0 = \hbar\omega + E_b$ clearly indicates the resonant excitation of the bound state.

By modifying the driving frequency and the potential parameters, multiple Fano resonances occur, as shown in Fig. 2(c). The number of Fano resonances depends on the number of bound states whose energy E_b is within the range $[-\hbar\omega, 0]$. For the potential parameters and ω used in Fig. 2(c), there exist three bound states $E_b^i \in [-\hbar\omega, 0]$ $(i = 1, 2, 3)$ as detailed in the Appendix, *i.e.*, $E_b^1 \approx -0.91\hbar\omega$, $E_b^2 \approx -0.64\hbar\omega$, $E_b^3 \approx -0.24\hbar\omega$. This gives rise to three Fano resonances at $E_b^i + \hbar\omega$ in the transmission spectrum as illustrated in Fig. 2(c).

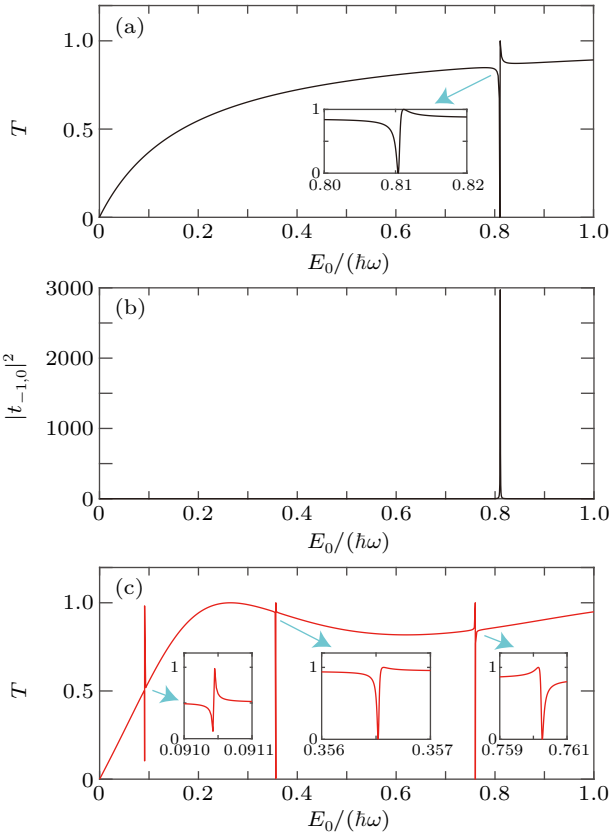


Fig. 2. Spectral transmittance T through a trapping potential subjected to a weak coherent driving (*i.e.*, $V(x,t) = V_0 + V_1\cos(\omega t)$, with $|V_1| < |V_0|$). All energy scales are given in the unit of $E_R = \hbar^2/(2\mu a^2)$, with a being typical length unit of the system. In our calculations, we fix the coherent driving amplitude $V_1 = 0.1E_R$, while varying the static potential parameters (V_0 and L) and the driving frequency ω. (a) Transmittance T as a function of the incident energy $E_0/(\hbar\omega)$ for $\hbar\omega = E_R$, $L = a$, $V_0 = -E_R$. (b) Transmission probability $|t_{-10}|^2$ in the $n = -1$ Floquet channel as a function of $E_0/(\hbar\omega)$. (c) T as a function of $E_0/(\hbar\omega)$ for $\hbar\omega = 4E_R$, $L = 4.19a$, and $V_0 = -4E_R$. In all plots, Floquet channels $\in [-5, 5]$ are accounted for in the numerical computation. In panels (a) and (c), the insets zoom in the resonance lineshapes.

5. Scattering from a purely incoherently driven potential

What will happen when, instead of a coherent driving, the static potential is subjected to a purely incoherent driving $V_2 \neq 0$? We address this question in this section. Mathematically, this corresponds to adding a purely imaginary term $-iV_2\sin(\omega t)$ on top of the otherwise static potential V_0.

We first choose $V_0 = -E_R$ and $\hbar\omega = E_R$ similar as in Fig. 2(a), so that without driving there exists one bound state within the range $[-\hbar\omega, 0]$. Like its coherent-driving counterpart, a transmission resonance [Fig. 3(a)] is found to occur at the incident energy $E_0 = E_b + \hbar\omega$. In contrast to Fig. 2(a), however, the Fano lineshape is reversed: the dip (peak) in Fig. 2(a) turns into a peak (dip) in Fig. 3(a).

Such a reversed lineshape cannot be achieved in the purely coherent driving case through modifying $V_1\cos(\omega t)$ to $V_1\sin(\omega t)$. Rather, this is likely induced by the purely incoherent nature of the driving: mathematically, an incoherent driving $\mathrm{i}V_2\sin(\omega t)$ can be seen as a coherent driving multiplied by "i". This multiplication does not change the resonant transition between the incident channel and the bound state, but introduces a relative phase shift $\pi/2$, which switches the sign of the Fano parameter[33,34] compared to the coherent counterpart, reversing the lineshape. This conjecture is supported by Fig. 3(b), where we choose the same V_0 and ω as Fig. 2(c), but now under the incoherent driving. We see that, still, three Fano resonances occur near $E_0 = E_{\rm b}^i + \hbar\omega$ $(i = 1,2,3)$, but each resonance lineshape (inset) is reversed compared to their counterpart in Fig. 2(c).

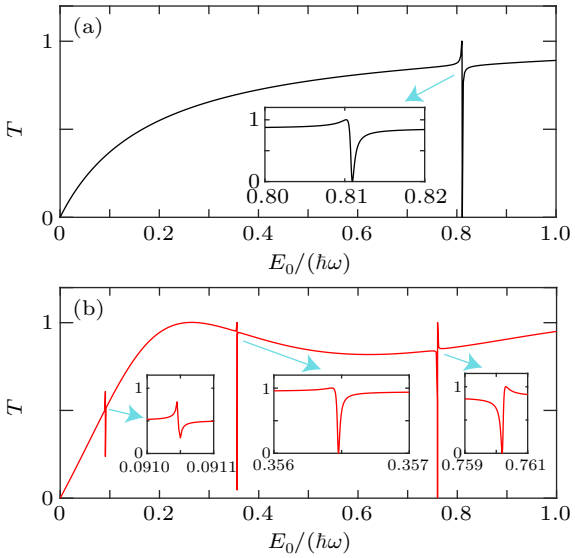


Fig. 3. Spectral transmittance T through a trapping potential subjected to a weak incoherent driving (*i.e.*, $V(x,t) = V_0 - \mathrm{i}V_2\sin(\omega t)$, with $|V_2| < |V_0|$). In our calculations, we fix the driving amplitude $V_2 = 0.1E_{\rm R}$, while varying the static potential parameters (V_0 and L) and the driving frequency ω. (a)–(b) Transmittance T as a function of the incident energy $E_0/(\hbar\omega)$ for (a) $\hbar\omega = E_{\rm R}$, $L = a$, and $V_0 = -E_{\rm R}$, and (b) $\hbar\omega = 4E_{\rm R}$, $L = 4.19a$, and $V_0 = -4E_{\rm R}$. In all plots, Floquet channels $\in [-5,5]$ are accounted for in the numerical computation. In panels (a) and (b), the insets zoom in the resonance lineshapes.

6. Scattering from a complex-driven potential

In this section, we consider the case when both coherent and incoherent periodic drivings are present. In Fig. 4, we illustrate the transmission spectrum, fixing other parameters to be the same as in Fig. 2(a). For $|V_2/V_1| < 1$, when the coherent driving dominates, we see that the transmission spectrum is qualitatively similar as Fig. 2(a). This includes the single Fano resonance near $E_0 = E_{\rm b} + \hbar\omega$, corresponding to the bound state with $E_{\rm b} \approx -0.19\hbar\omega$, as well as the similar lineshape as in Fig. 2(a), with the dip followed by the peak (yellow curve). In contrast, for $|V_2/V_1| > 1$, when the incoherent driving dominates, we see that the Fano lineshape is reversed (purple curve).

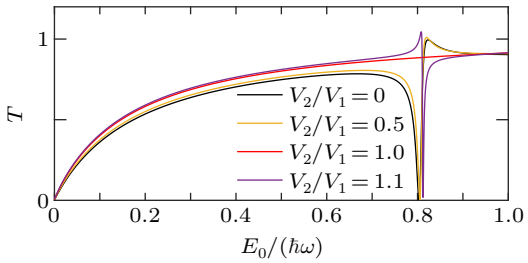


Fig. 4. Spectral transmittance T as a function of $E_0/(\hbar\omega)$ for various V_2/V_1. We take $\hbar\omega = E_{\rm R}$, $L = a$, $V_0 = -E_{\rm R}$, and $V_1 = 0.5E_{\rm R}$. Floquet channels $\in [-5,5]$ are taken into account in the numerical calculations.

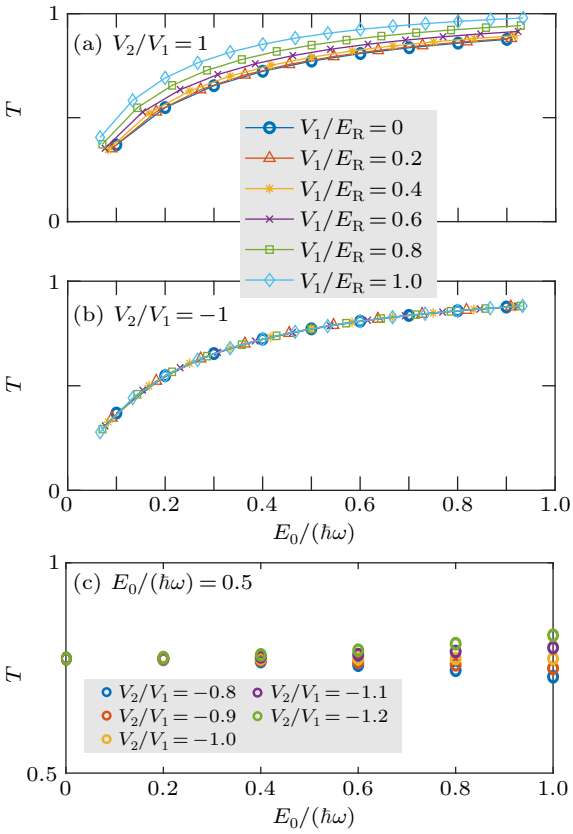


Fig. 5. Behavior of spectral transmittance T at $V_2 = \pm V_1$. (a), (b) Spectral transmittance T as a function of $E_0/(\hbar\omega)$ for various amplitude V_1, when (a) $V_2 = V_1$ and (b) $V_2 = -V_1$. For other parameters, we use $\hbar\omega = E_{\rm R}$, $L = a$, and $V_0 = -E_{\rm R}$. (c) T for $V_1/E_{\rm R} = 0, 0.2, 0.4, 0.6, 0.8, 1$, when $V_2/V_1 = -0.8, -0.9, -1, 1.1, 1.2$. We choose $E_0/(\hbar\omega) = 0.5$. In all plots, Floquet channels $\in [-10,10]$ are accounted for in the numerical calculations.

It turns out that when $V_1 = V_2$, the Fano resonance disappears (see Fig. 4). To understand this phenomenon, we note that when $V_1 = V_2$, one can rewrite $V(x,t) = V_0 + V_1\,\mathrm{e}^{-\mathrm{i}\omega t}$ $(|x| < L/2)$. Such a driving couples the Floquet channel n with the channel $n+1$, but not the channel $n-1$, *i.e.*, the coupling is upward nonreciprocal in the frequency domain. This means that when the particle interacts with the potential $V(x,t)$, it can only absorb $n = 1,2,\ldots$ energy quanta to jump into the Floquet channels with higher energies $E_0 + n\hbar\omega$, whereas the reciprocal processes involving emissions of energy quanta to drop to the lower-energy channels are absent. Hence the resonance of an incident particle with the bound state cannot occur, explaining the disappearance of the resonant transmission. In ad-

dition, for $V_1 = V_2$, we anticipate that when increasing V_1, the transmittance increases due to the growing number of (higher-energy) channels that contribute to the transmission, as seen in Fig. 5(a).

As well, for $V_1 = -V_2$, we have $V(x,t) = V_0 + V_1 \mathrm{e}^{\mathrm{i}\omega t}$ ($|x| < L/2$), and the transmission emission is anticipated to disappear due to the nonreciprocal coupling of Floquet channels, as shown in Fig. 5(b). However, the transmission exhibits different behavior compared to the case $V_1 = V_2$. The $V(x,t) = V_0 + V_1 \mathrm{e}^{\mathrm{i}\omega t}$ ($|x| < L/2$) couples Floquet channels in the frequency domain in a downward nonreciprocal fashion, *i.e.*, channel n is coupled only to channel $n-1$. As such, transitions from the incident channels to higher energy channels via the absorption of $n\hbar\omega$ are absent, and an incident particle can only emit $n = 1, 2, \ldots$ energy quanta to jump into the channels with energies $E_0 - n\hbar\omega < 0$. Since these lower-energy channels do not support propagating modes and thus do not contribute to the transmission, the transmission is independent of the specific value of V_1, as if there is no driving at all, as demonstrated in Fig. 5(b), supplemented with Fig. 5(c) for the transmission behavior in the vicinity of $V_1 = -V_2$.

7. Concluding discussion

In summary, we have investigated the 1D scattering of a particle off a $\mathcal{PT}$-symmetric, oscillating potential. Based on the Floquet theory, we have derived the scattering matrix and calculated the transmittance. For a potential subjected to a purely incoherent periodic driving, we find the bound-state induced Fano resonance in the transmission spectrum; however, the incoherent nature of the driving gives rise to a reversed Fano lineshape compared to the coherent-driving counterpart. Intriguingly, when the coherent and incoherent drivings have equal amplitude, we find the transmission resonances disappear, which originates from the non-reciprocal coupling of Floquet channels in the frequency domain. In particular, we find that when the complex driving fields are such that makes the downward frequency conversion process absent, increasing the driving amplitude enhances the transmission, whereas when the upward conversion is absent, the incident particle transmits through the potential as if there is no driving at all.

We remark that the cases $|V_1| = |V_2|$ are intimately connected to the exceptional point (EP) of a Floquet matrix in the frequency domain. An intuitive picture is best illustrated for $V_0 = 0$, in the absence of the static trap, so that the system is only subjected to a $\mathcal{PT}$-symmetric driving. In this case, $|V_1| = |V_2|$ exactly corresponds to the EP of the Floquet transmission matrix $\boldsymbol{T}$, which at this point well approximates the Jordan standard form and can be interpreted as a synthetic lattice with nonreciprocal nearest neighbor couplings. Our manuscript has focused on the case $|V_0| > |V_1|, |V_2|$, since we are interested in the scenario where there exists static bound state. Nonetheless, although the $\boldsymbol{T}$ matrix does not take the Jordan standard form, the aforementioned EP physics still leaves a fingerprint in the transmission behavior, namely through the significant changes in the Fano resonance lineshapes across the point $|V_1| = |V_2|$: When $|V_1| > |V_2|$, the Fano profile is a dip followed by a peak; when $|V_1| < |V_2|$, the Fano profile is a peak followed by a dip; exactly at $|V_1| = |V_2|$, the Fano resonance disappears.

Based on the current understandings, interesting directions in the future include the design of scattering matrix in the context of lattice models, such as non-Hermitian topological arrays,[2,35–43] as well as to the case when there exists non-equilibrium bound states.[23]

Appendix A: Derivation of the scattering matrix

In this section, we present a detailed derivation for the Floquet $\boldsymbol{S}$ matrix in Eq. (15) of the main text, extending the approach in Ref. [23] to the case with $\mathcal{PT}$-symmetric driving.

Our starting point is Eqs. (1)–(5). In the regions $|x| > L/2$, accounting for incoming waves also from the right, we have

$$\phi = \sum_{n=-\infty}^{\infty} \left(A_n^{\mathrm{i}} \mathrm{e}^{\mathrm{i}k_n x} + A_n^{\mathrm{o}} \mathrm{e}^{-\mathrm{i}k_n x}\right) \mathrm{e}^{-\mathrm{i}n\omega t}, \quad (x < -L/2), \tag{A1}$$

$$\phi = \sum_{n=-\infty}^{\infty} \left(B_n^{\mathrm{i}} \mathrm{e}^{-\mathrm{i}k_n x} + B_n^{\mathrm{o}} \mathrm{e}^{\mathrm{i}k_n x}\right) \mathrm{e}^{-\mathrm{i}n\omega t}, \quad (x > L/2), \tag{A2}$$

where A_n^{i} (B_n^{i}) denote the amplitudes of the wave in the n-th Floquet channel from the left (right). In the regions $|x| < L/2$, the solution is still given by Eq. (11) in the main text.

Next, we exploit the boundary conditions to connect the wavefunctions in different regimes. At $x = -L/2$, we have

$$\begin{aligned} & A_n^{\mathrm{i}} \mathrm{e}^{-\mathrm{i}k_n L/2} + A_n^{\mathrm{o}} \mathrm{e}^{\mathrm{i}k_n L/2} \\ = & \sum_m \left(a_m \mathrm{e}^{-\mathrm{i}q_m L/2} + b_m \mathrm{e}^{\mathrm{i}q_m L/2}\right) h_{n-m}, \end{aligned} \tag{A3}$$

$$\begin{aligned} & \mathrm{i}k_n (A_n^{\mathrm{i}} \mathrm{e}^{-\mathrm{i}k_n L/2} - A_n^{\mathrm{o}} \mathrm{e}^{\mathrm{i}k_n L/2}) \\ = & \sum_m \mathrm{i}q_m \left(a_m \mathrm{e}^{-\mathrm{i}q_m L/2} - b_m \mathrm{e}^{\mathrm{i}q_m L/2}\right) h_{n-m}, \end{aligned} \tag{A4}$$

where h_{n-m} is defined in Eq. (12). Similarly, at $x = L/2$, we have

$$\begin{aligned} & B_n^{\mathrm{i}} \mathrm{e}^{-\mathrm{i}k_n L/2} + B_n^{\mathrm{o}} \mathrm{e}^{\mathrm{i}k_n L/2} \\ = & \sum_m \left(a_m \mathrm{e}^{\mathrm{i}q_m L/2} + b_m \mathrm{e}^{-\mathrm{i}q_m L/2}\right) h_{n-m}, \end{aligned} \tag{A5}$$

$$\begin{aligned} & -\mathrm{i}k_n (B_n^{\mathrm{i}} \mathrm{e}^{-\mathrm{i}k_n L/2} - B_n^{\mathrm{o}} \mathrm{e}^{\mathrm{i}k_n L/2}) \\ = & \sum_m \mathrm{i}q_m \left(a_m \mathrm{e}^{\mathrm{i}q_m L/2} - b_m \mathrm{e}^{-\mathrm{i}q_m L/2}\right) h_{n-m}. \end{aligned} \tag{A6}$$

From Eqs. (A3) and (A5), we express the outgoing amplitudes A_n^{o} and B_n^{o} as

$$\begin{aligned} A_n^{\mathrm{o}} = & \sum_m (a_m \mathrm{e}^{-\mathrm{i}q_m L/2} + b_m \mathrm{e}^{\mathrm{i}q_m L/2}) h_{n-m} \mathrm{e}^{-\mathrm{i}k_n L/2} \\ & - A_n^{\mathrm{i}} \mathrm{e}^{-\mathrm{i}k_n L}, \end{aligned} \tag{A7}$$

$$\begin{aligned} B_n^{\mathrm{o}} = & \sum_m (a_m \mathrm{e}^{\mathrm{i}q_m L/2} + b_m \mathrm{e}^{-\mathrm{i}q_m L/2}) h_{n-m} \mathrm{e}^{-\mathrm{i}k_n L/2} \\ & - B_n^{\mathrm{i}} \mathrm{e}^{-\mathrm{i}k_n L}. \end{aligned} \tag{A8}$$

Substituting above expressions into Eqs. (A4) and (A6) respectively, we obtain

$$2k_nA_n^{\rm i}\,{\rm e}^{-{\rm i}k_nL/2} = \sum_m\Big[(k_n+q_m)a_m\,{\rm e}^{-{\rm i}q_mL/2} +(k_n-q_m)b_m\,{\rm e}^{{\rm i}q_mL/2}\Big]h_{n-m}, \tag{A9}$$

$$2k_nB_n^{\rm i}\,{\rm e}^{-{\rm i}k_nL/2} = \sum_m\Big[(k_n-q_m)a_m\,{\rm e}^{{\rm i}q_mL/2} +(k_n+q_m)b_m\,{\rm e}^{-{\rm i}q_mL/2}\Big]h_{n-m}. \tag{A10}$$

Addition of Eqs. (A9) and (A10) gives the following infinite matrix equation:

$$2k_n(A_n^{\rm i}\pm B_n^{\rm i})\,{\rm e}^{-{\rm i}k_nL/2} = \sum_m(a_m\pm b_m)\Big[(k_n+q_m) \times{\rm e}^{-{\rm i}q_mL/2}\pm(k_n-q_m)\,{\rm e}^{{\rm i}q_mL/2}\Big]h_{n-m}. \tag{A11}$$

For clarity, let us introduce the following notations:

$$\begin{aligned}
&C_m^{\pm} = a_m\pm b_m,\\
&(\boldsymbol{M}_{\rm s}^{\pm})_{n,m} = \Big[(k_n+q_m)\,{\rm e}^{-{\rm i}q_mL/2}\pm(k_n-q_m)\,{\rm e}^{{\rm i}q_mL/2}\Big]h_{n-m},\\
&(\boldsymbol{M}_{\rm r})_{n,m} = 2k_n\,{\rm e}^{-{\rm i}k_nL/2}\delta_{n,m},\\
&(\boldsymbol{M}_{\rm c}^{\pm})_{n,m} = {\rm e}^{-{\rm i}(k_n\pm q_m)L/2}h_{n-m},\\
&(\boldsymbol{M}_i)_{n,m} = {\rm e}^{-{\rm i}k_nL}\delta_{n,m}.
\end{aligned}$$

Using these notations, equation (A11) can be recast into a compact form as

$$\boldsymbol{C}^{\pm} = \left(\boldsymbol{M}_{\rm s}^{\pm}\right)^{-1}\cdot\boldsymbol{M}_{\rm r}\cdot\left(\boldsymbol{A}^{\rm i}\pm\boldsymbol{B}^{\rm i}\right). \tag{A12}$$

The coefficients a_m and b_m can thus be straightforwardly found as

$$\begin{aligned}
\boldsymbol{a} &= \frac{1}{2}\Big[\left(\boldsymbol{M}_{\rm s}^{+}\right)^{-1}\cdot\boldsymbol{M}_{\rm r}\cdot\left(\boldsymbol{A}^{\rm i}+\boldsymbol{B}^{\rm i}\right) +\left(\boldsymbol{M}_{\rm s}^{-}\right)^{-1}\cdot\boldsymbol{M}_{\rm r}\cdot\left(\boldsymbol{A}^{\rm i}-\boldsymbol{B}^{\rm i}\right)\Big]\\
&= \left[\frac{\left(\boldsymbol{M}_{\rm s}^{+}\right)^{-1}+\left(\boldsymbol{M}_{\rm s}^{-}\right)^{-1}}{2}\right]\cdot\boldsymbol{M}_{\rm r}\cdot\boldsymbol{A}^{\rm i} +\left[\frac{\left(\boldsymbol{M}_{\rm s}^{+}\right)^{-1}-\left(\boldsymbol{M}_{\rm s}^{-}\right)^{-1}}{2}\right]\cdot\boldsymbol{M}_{\rm r}\cdot\boldsymbol{B}^{\rm i},\\
\boldsymbol{b} &= \left[\frac{\left(\boldsymbol{M}_{\rm s}^{+}\right)^{-1}-\left(\boldsymbol{M}_{\rm s}^{-}\right)^{-1}}{2}\right]\cdot\boldsymbol{M}_{\rm r}\cdot\boldsymbol{A}^{\rm i} +\left[\frac{\left(\boldsymbol{M}_{\rm s}^{+}\right)^{-1}+\left(\boldsymbol{M}_{\rm s}^{-}\right)^{-1}}{2}\right]\cdot\boldsymbol{M}_{\rm r}\cdot\boldsymbol{B}^{\rm i}.
\end{aligned}$$

Using the above equation for the coefficients a_m and b_m, we obtain from Eqs. (A7) and (A8) that the outgoing wave-amplitudes in the left and right are, respectively,

$$\begin{aligned}
\boldsymbol{A}^{\rm o} &= \boldsymbol{M}_{\rm c}^{+}\cdot\boldsymbol{a}+\boldsymbol{M}_{\rm c}^{-}\cdot\boldsymbol{b}-\boldsymbol{M}_{\rm i}\cdot\boldsymbol{A}^{\rm i}\\
&= \left(\frac{1}{2}\Big\{\boldsymbol{M}_{\rm c}^{+}\cdot\Big[\left(\boldsymbol{M}_{\rm s}^{+}\right)^{-1}+\left(\boldsymbol{M}_{\rm s}^{-}\right)^{-1}\Big] +\boldsymbol{M}_{\rm c}^{-}\cdot\Big[\left(\boldsymbol{M}_{\rm s}^{+}\right)^{-1}-\left(\boldsymbol{M}_{\rm s}^{-}\right)^{-1}\Big]\Big\}\cdot\boldsymbol{M}_{\rm r}-\boldsymbol{M}_{\rm i}\right)\cdot\boldsymbol{A}^{\rm i}\\
&\quad+\left(\frac{1}{2}\Big\{\boldsymbol{M}_{\rm c}^{+}\cdot\Big[\left(\boldsymbol{M}_{\rm s}^{+}\right)^{-1}-\left(\boldsymbol{M}_{\rm s}^{-}\right)^{-1}\Big] +\boldsymbol{M}_{\rm c}^{-}\cdot\Big[\left(\boldsymbol{M}_{\rm s}^{+}\right)^{-1}+\left(\boldsymbol{M}_{\rm s}^{-}\right)^{-1}\Big]\Big\}\cdot\boldsymbol{M}_{\rm r}\right)\cdot\boldsymbol{B}^{\rm i}\\
&= \boldsymbol{M}_{AA}\cdot\boldsymbol{A}^{\rm i}+\boldsymbol{M}_{AB}\cdot\boldsymbol{B}^{\rm i},
\end{aligned} \tag{A13}$$

$$\begin{aligned}
\boldsymbol{B}^{\rm o} &= \boldsymbol{M}_{\rm c}^{-}\cdot\boldsymbol{a}+\boldsymbol{M}_{\rm c}^{+}\cdot\boldsymbol{b}-\boldsymbol{M}_{\rm i}\cdot\boldsymbol{B}^{\rm i}\\
&= \left(\frac{1}{2}\Big\{\boldsymbol{M}_{\rm c}^{-}\cdot\Big[\left(\boldsymbol{M}_{\rm s}^{+}\right)^{-1}+\left(\boldsymbol{M}_{\rm s}^{-}\right)^{-1}\Big] +\boldsymbol{M}_{\rm c}^{+}\cdot\Big[\left(\boldsymbol{M}_{\rm s}^{+}\right)^{-1}-\left(\boldsymbol{M}_{\rm s}^{-}\right)^{-1}\Big]\Big\}\cdot\boldsymbol{M}_{\rm r}\right)\cdot\boldsymbol{A}^{\rm i}\\
&\quad+\left(\frac{1}{2}\Big\{\boldsymbol{M}_{\rm c}^{-}\cdot\Big[\left(\boldsymbol{M}_{\rm s}^{+}\right)^{-1}-\left(\boldsymbol{M}_{\rm s}^{-}\right)^{-1}\Big] +\boldsymbol{M}_{\rm c}^{+}\cdot\Big[\left(\boldsymbol{M}_{\rm s}^{+}\right)^{-1}+\left(\boldsymbol{M}_{\rm s}^{-}\right)^{-1}\Big]\Big\}\cdot\boldsymbol{M}_{\rm r}-\boldsymbol{M}_{\rm i}\right)\cdot\boldsymbol{B}^{\rm i}\\
&= \boldsymbol{M}_{BA}\cdot\boldsymbol{A}^{\rm i}+\boldsymbol{M}_{BB}\cdot\boldsymbol{B}^{\rm i},
\end{aligned} \tag{A14}$$

where we have

$$\boldsymbol{M}_{AB}=\boldsymbol{M}_{BA} = \frac{1}{2}\Big\{\boldsymbol{M}_{\rm c}^{-}\cdot\Big[\left(\boldsymbol{M}_{\rm s}^{+}\right)^{-1}+\left(\boldsymbol{M}_{\rm s}^{-}\right)^{-1}\Big] +\boldsymbol{M}_{\rm c}^{+}\cdot\Big[\left(\boldsymbol{M}_{\rm s}^{+}\right)^{-1}-\left(\boldsymbol{M}_{\rm s}^{-}\right)^{-1}\Big]\Big\}\cdot\boldsymbol{M}_{\rm r}.$$

Finally, collecting Eqs. (A13) and (A14), we arrive at the general expression

$$\begin{pmatrix}\boldsymbol{A}^{\rm o}\\ \boldsymbol{B}^{\rm o}\end{pmatrix} = \begin{pmatrix}\boldsymbol{M}_{AA} & \boldsymbol{M}_{AB}\\ \boldsymbol{M}_{BA} & \boldsymbol{M}_{BB}\end{pmatrix}\begin{pmatrix}\boldsymbol{A}^{\rm i}\\ \boldsymbol{B}^{\rm i}\end{pmatrix},$$

which is Eq. (15) in the main text.

Appendix B: Bound state in the absence of driving

In this section, we solve the bound states in the static case without driving (*i.e.*, $V_1=0$ and $V_2=0$). Assuming $V_0<0$, we look for the bound state solution with the energy $E<0$ following the standard procedures.

Outside the potential well ($|x|>L/2$), the stationary Schrödinger equation reads

$$\frac{\partial^2}{\partial x^2}\psi(x) = -\frac{2\mu E}{\hbar^2}\psi(x) = \beta^2\psi(x),$$

with $\beta=\sqrt{-2\mu E}/\hbar$. Further considering the boundary conditions $\psi(\pm\infty)=0$, we have

$$\psi(x) = \begin{cases} A\,{\rm e}^{-\beta x}, & (x>L/2),\\ B\,{\rm e}^{\beta x}, & (x<-L/2),\end{cases}$$

where A and B are to be determined in the following.

In the trapping potential (*i.e.*, $|x|<L/2$), we have

$$\frac{\partial^2}{\partial x^2}\psi(x) = \frac{-2\mu(E-V_0)}{\hbar^2}\psi(x) = -k^2\psi(x),$$

with $k=\sqrt{2\mu(E-V_0)}/\hbar$. Note the solution has definite parity.

(i) For the even parity solution $\psi(x) \propto \cos(kx)$, the continuity condition at $x = L/2$ gives

$$(\cos(kx))'|_{x=L/2} = -(A\,\mathrm{e}^{-\beta x})'|_{x=L/2},$$
$$\cos(kx)|_{x=L/2} = -A\,\mathrm{e}^{-\beta x}|_{x=L/2}.$$

This gives $\beta = k\tan(kL/2)$, which can be rewritten as

$$\eta = \xi\tan(\xi), \tag{B1}$$

where we have defined $\xi = kL/2$, $\eta = \beta L/2$. According to the definitions of k and β, we further have

$$\xi^2 + \eta^2 = (kd/2)^2 + (\beta d/2)^2 = -\frac{\mu V_0 L^2}{2\hbar^2}. \tag{B2}$$

We numerically find the even-parity bound states via the graphic solutions shown in Fig. B1, as represented by the intersections of the function (B1) (blue curve) and the function (B2) (red curve).

(ii) For the odd parity solution $\psi(x) = \sin kx$, the procedures are similar as above, except that Eq. (B1) is replaced by

$$\eta = -\xi\cot\xi. \tag{B3}$$

Intersections of the function (B2) (red curve) with Eq. (B3) (black curve) provide us solutions of the bound states with the odd parity; see Fig. B1.

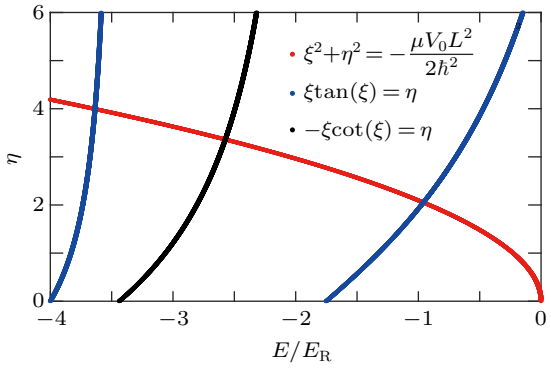


Fig. B1. Graphic solutions for the bound states in the presence of a trapping potential with $L = 4.19a$ and $V_0 = -4E_{\mathrm{R}}$. The blue curve denotes the function (B1), the black curve denotes the function (B3), while the red curve denotes the function (B2). Intersections of the red curve with the blue (black) curve gives the energies E of the even-parity (odd-parity) bound-states. Here, three bound states are shown whose energy E is in the energy regime $[-4E_{\mathrm{R}}, 0]$; their energies are read off as $E \approx -0.96E_{\mathrm{R}}$, $E \approx -2.57E_{\mathrm{R}}$, and $E \approx -3.64E_{\mathrm{R}}$, respectively.

Acknowledgments

Project supported by the National Key Research and Development Program of China (Grant No. 2017YFA0304203), the National Natural Science Foundation of China (Grant No. 11874038), the Zhejiang Provincial Natural Science Foundation (Grant No. LZ21A040001), the National Natural Science Foundation of China (Grant No. 12074344), and the Key Projects of the Natural Science Foundation of China (Grant No. 11835011).

References

[1] Bender C M and Boettcher S 1998 *Phys. Rev. Lett.* **80** 5243
[2] Bergholtz E J, Budich J C and Kunst F K 2021 *Rev. Mod. Phys.* **93** 015005
[3] Bender C M, Berntson B K, Parker D and Samuel E 2013 *Am. J. Phys.* **81** 173
[4] Guo A, Salamo G J, Duchesne D, Morandotti R, Volatier-Ravat M, Aimez V, Siviloglou G A and Christodoulides D N 2009 *Phys. Rev. Lett.* **103** 093902
[5] Rüter C E, Makris K G, El-Ganainy R, Christodoulides D N, Segev M and Kip D 2010 *Nat. Phys.* **6** 192
[6] Feng L, Xu Y L, Fegadolli W S, Lu M H, Oliveira J E B, Almeida V R, Chen Y F and Scherer A 2013 *Nat. Mater.* **12** 108
[7] Chang L, Jiang X, Hua S, Yang C, Wen J, Jiang L, Li G, Wang G and Xiao M 2014 *Nat. Photon.* **8** 524
[8] Peng B, Özdemir Ş K, Lei F, Monifi F, Gianfreda M, Long G L, Fan S, Nori F, Bender C M and Yang L 2014 *Nat. Phys.* **10** 394
[9] Zhang F, Feng Y, Chen X, Ge L and Wan W 2020 *Phys. Rev. Lett.* **124** 053901
[10] Zhao J, Liu Y, Wu L, Duan C K, Liu Y X and Du J 2020 *Phys. Rev. Appl.* **13** 014053
[11] Feng L, Wong Z J, Ma R M, Wang Y and Zhang X 2014 *Science* **346** 972
[12] Hodaei H, Miri M A, Heinrich M, Christodoulides D N and Khajavikhan M 2014 *Science* **346** 975
[13] Jing H, Özdemir S K, Lü X Y, Zhang J, Yang L and Nori F 2014 *Phys. Rev. Lett.* **113** 053604
[14] Lü X Y, Jing H, Ma J Y and Wu Y 2015 *Phys. Rev. Lett.* **114** 253601
[15] Schönleber D W, Eisfeld A and El-Ganainy R 2016 *New J. Phys.* **18** 045014
[16] Jing H, Özdemir Ş K, Lü H and Nori F 2017 *Sci. Rep.* **7** 3386
[17] Støvneng J A and Hauge E H 1989 *J. Stat. Phys.* **57** 841
[18] Wagner M 1994 *Phys. Rev. B* **49** 16544
[19] Wagner M 1995 *Phys. Rev. A* **51** 798
[20] Saraga D S and Bianchi M S de 1997 *Helv. Phys. Acta* **70** 751
[21] Sun Q f, Wang J and Lin T H 1998 *Phys. Rev. B* **58** 13007
[22] Burmeister G and Maschke K 1998 *Phys. Rev. B* **57** 13050
[23] Li W and Reichl L E 1999 *Phys. Rev. B* **60** 15732
[24] Kouwenhoven L P, Jauhar S, Orenstein J, McEuen P L, Nagamune Y, Motohisa J and Sakaki H 1994 *Phys. Rev. Lett.* **73** 3443
[25] Blick R H, Haug R J, Weide D W van der, Klitzing K von and Eberl K 1995 *Appl. Phys. Lett.* **67** 3924
[26] Drexler H, Scott J S, Allen S J, Campman K L and Gossard A C 1995 *Appl. Phys. Lett.* **67** 2816
[27] Keay B J, Allen S J, Jr, Galán J, Kaminski J P, Campman K L, Gossard A C, Bhattacharya U and Rodwell M J W 1995 *Phys. Rev. Lett.* **75** 4098
[28] Thuberg D, Reyes S A and Eggert S 2016 *Phys. Rev. B* **93** 180301
[29] Mostafazadeh A 2009 *Phys. Rev. Lett.* **102** 220402
[30] Longhi S 2017 *Europhys. Lett.* **117** 10005
[31] Shobe K, Kuramoto K, Imura K I and Hatano N 2021 *Phys. Rev. Research* **3** 013223
[32] Shirley J H 1965 *Phys. Rev.* **138** B979
[33] Fano U 1961 *Phys. Rev.* **124** 1866
[34] Limonov M F, Rybin M V, Poddubny A N and Kivshar Y S 2017 *Nat. Photon.* **11** 543
[35] Yao S and Wang Z 2018 *Phys. Rev. Lett.* **121** 086803
[36] Kunst F K, Edvardsson E, Budich J C and Bergholtz E J 2018 *Phys. Rev. Lett.* **121** 026808
[37] Gong Z, Ashida Y, Kawabata K, Takasan K, Higashikawa S and Ueda M 2018 *Phys. Rev. X* **8** 031079
[38] Zhou H, Peng C, Yoon Y, Hsu C W, Nelson K A, Fu L, Joannopoulos J D, Soljačić M and Zhen B 2018 *Science* **359** 1009
[39] Kawabata K, Shiozaki K, Ueda M and Sato M 2019 *Phys. Rev. X* **9** 041015
[40] Xiao L, Deng T, Wang K, Zhu G, Wang Z, Yi W and Xue P 2020 *Nat. Phys.* **16** 761
[41] Wanjura C C, Brunelli M and Nunnenkamp A 2020 *Nat. Commun.* **11** 3149
[42] Hu B, Zhang Z, Zhang H, Zheng L, Xiong W, Yue Z, Wang X, Xu J, Cheng Y, Liu X and Christensen J 2021 *Nature* **597** 655
[43] Liang Q, Xie D, Dong Z, Li H, Li H, Gadway B, Yi W and Yan B 2022 *Phys. Rev. Lett.* **129** 070401